Available online at www.sciencedirect.com
ScienceDirect
Journal of the European Ceramic Society 28 (2008) 1169–1176
www.elsevier.com/locate/jeurceramsoc

On the reorientation of $ZrTiO_4$ particles during reactive sintering of TiO_2–ZrO_2

K.C. Yang [1], P. Shen *, D. Gan

Institute of Materials Science and Engineering, National Sun Yat-sen University, Kaohsiung, Taiwan, ROC

Received 1 July 2007; received in revised form 17 September 2007; accepted 30 September 2007
Available online 19 November 2007

Abstract

ZrO_2 and TiO_2 powders were reactively sintered at 1600 °C in air to form orthorhombic $ZrTiO_4$ (α-PbO_2-type structure, denoted as α) particles in the matrix of Zr-dissolved TiO_2 (rutile denoted as r) grains following the preferred epitaxial relationship $[0\,\bar{1}\,0]_\alpha//[0\,\bar{1}\,1]_r$; $(0\,0\,1)_\alpha//(0\,1\,1)_r$ (i.e. $[1\,0\,0]_\alpha//[1\,0\,0]_r$; $(0\,0\,1)_\alpha//(0\,1\,1)_r$) as determined by analytical electron microscopy. The epitaxial $ZrTiO_4$ particles formed laths with $(1\,0\,1)_\alpha/(2\,1\,1)_r$ habit plane having fair match of oxygen atoms and beneficial low interfacial energy. The reorientation of the confined particles in the composites can be reasonably explained by Brownian rotation of the nonepitaxial intergranular particles and the reactive sintering process that facilitated the rotation of the particles about to detach from the grain boundaries.

Keywords: Reorientation; $ZrTiO_4$; Reactive sintering; TEM; Brownian motion

1. Introduction

The motivation of this research is to prove by experiments that Brownian rotation is feasible for the $ZrTiO_4$ (space group *Pbcn* with α-PbO_2-type structure) particles reactively sintered and then confined within Zr-dissolved TiO_2 grains having rutile-type structure (space group $P4_2/mnm$).

In previous annealing studies of cubic oxide composites prepared by solid-state sintering, e.g. $Ni_{1-x}O$/yttria partially stabilized zirconia (Y-PSZ),[1] $Ni_{1-x}O/NiAl_2O_4$,[2] and $Co_{1-x}O$/Y-PSZ,[3] we have proved that intragranular particles can change orientation until they reach epitaxial relationships with respect to the host grains. A relatively high homologous temperature (T/T_m where T_m is melting point in Kelvin) for the $Ni_{1-x}O/NiAl_2O_4$,[2] and $Co_{1-x}O$/Y-PSZ composites[3] resulted in a faster orientation change and more significant coalescence of the particles than the $Ni_{1-x}O$/Y-PSZ composite at a specified annealing temperature of 1600 °C.[1] Reorientation of the intragranular particles in these composites has little to do with sintering,[4] diffusion induced recrystallization[5] or dynamic recrystallization,[6] but can be reasonably explained by rotation of the particles above a critical temperature for anchorage release at the interface with respect to the host grain.[1–3]

In such a thermally activated rotation process of the intragranular particles, Brownian motion of the particles in terms of interfacial diffusion of atoms was suggested to happen[1–3] as for the case of fcc metal crystallites migrating and rotating on single crystal substrate, KCl(1 0 0) with or without steps.[7–12] The size and temperature dependence of diffusivity of the crystallites has been measured over KCl(1 0 0)[7] and found to be in accordance with Brownian-type motion of the crystallites in terms of interfacial diffusion of atoms from leading edge to trailing edge of the crystallites. Einstein's molecular theory of heat,[13] Eyring's transition-state model[14] and frictional force at a viscous interface were thus adopted to formulate the diffusivity equation of the crystallite over the single crystal substrate.[8–10] The size dependence of orientation change of intragranular particles was also verified by annealing experiments for the case of $Co_{1-x}O$ particles in Y-PSZ grain.[3]

Recently, oxidation-decomposition facilitated Brownian rotation of crystallites in the $(Ni_mCo_{1-m})_{1-\delta}O$ polycrystals was studied.[15] We further showed here that Brownian rotation of

* Corresponding author. Fax: +886 7 5254099.
E-mail address: pshen@mail.nsysu.edu.tw (P. Shen).
[1] Present address: Steel and Aluminium R&D Department, China Steel Corporation, Kaohsiung, Taiwan, ROC.

0955-2219/$ – see front matter © 2007 Elsevier Ltd. All rights reserved.
doi:10.1016/j.jeurceramsoc.2007.09.049

compound $ZrTiO_4$ particles readily occurred during their reactive sintering and incorporation into Zr-dissolved rutile grains until the two phases reached specific crystallographic relationship with a beneficial low interfacial energy.

2. Experimental

Powders of reagent grade ZrO_2 (Cerac, 99.9%, 3 μm in size) and TiO_2 (Aldrich, 99.9%, 5 μm in size) in 1:4 molar ratio (denoted as Z20T80) were mixed by a magnetic stirrer in ethanol at 50 °C for 2 h. The slurry was dried in an oven at 70 °C and ground with an agate mortar and pestle. The specimens were dry-pressed at 650 MPa to form pellets ca. 5 mm in diameter and 2 mm in thickness. The dry-pressed pellets were reactively sintered at 1600 °C for 0.5–36 h, in air and then air-quenched or furnace cooled to room temperature. For a better understanding of the reactions of phases, the pellets were also fired at 1400 or 1500 °C for 1 h in air and then air quenched. The fired specimens were polished by SiC sand paper and then diamond paste, followed by thermally etching to reveal grain boundaries of the sintered composites.

X-ray diffraction (XRD, Cu Kα, 40 kV, 30 mA) and least-squares refinement of the d-spacings were used to determine the lattice parameters of the $ZrTiO_4$ and Zr-dissolved TiO_2 in the fired composites. Scanning electron microscopy (SEM, JSM-

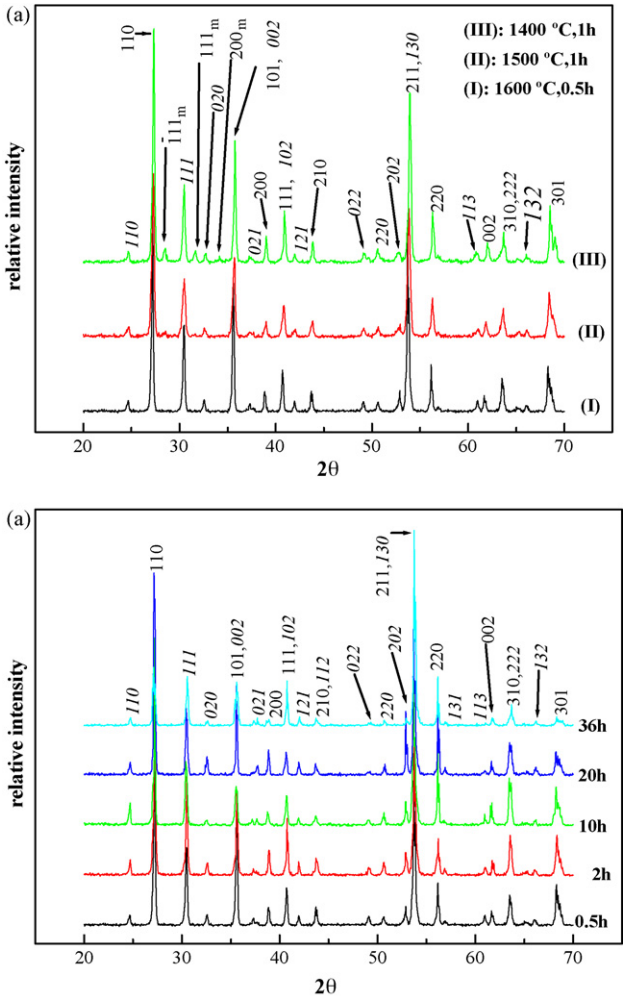

Fig. 1. XRD traces of the Z20T80 composites fired at various conditions showing Zr-dissolved rutile (denoted as ($h\,k\,l$)), $ZrTiO_4$ with α-PbO_2-type structure (denoted as italic ($h\,k\,l$)) and relic m-ZrO_2 (denoted as $(h\,k\,l)_m$). (a) short (0.5 h or 1 h) firing at 1400–1600 °C and then air quenched; (b) isothermal firing at 1600 °C for 0.5–36 h followed by air-quenching.

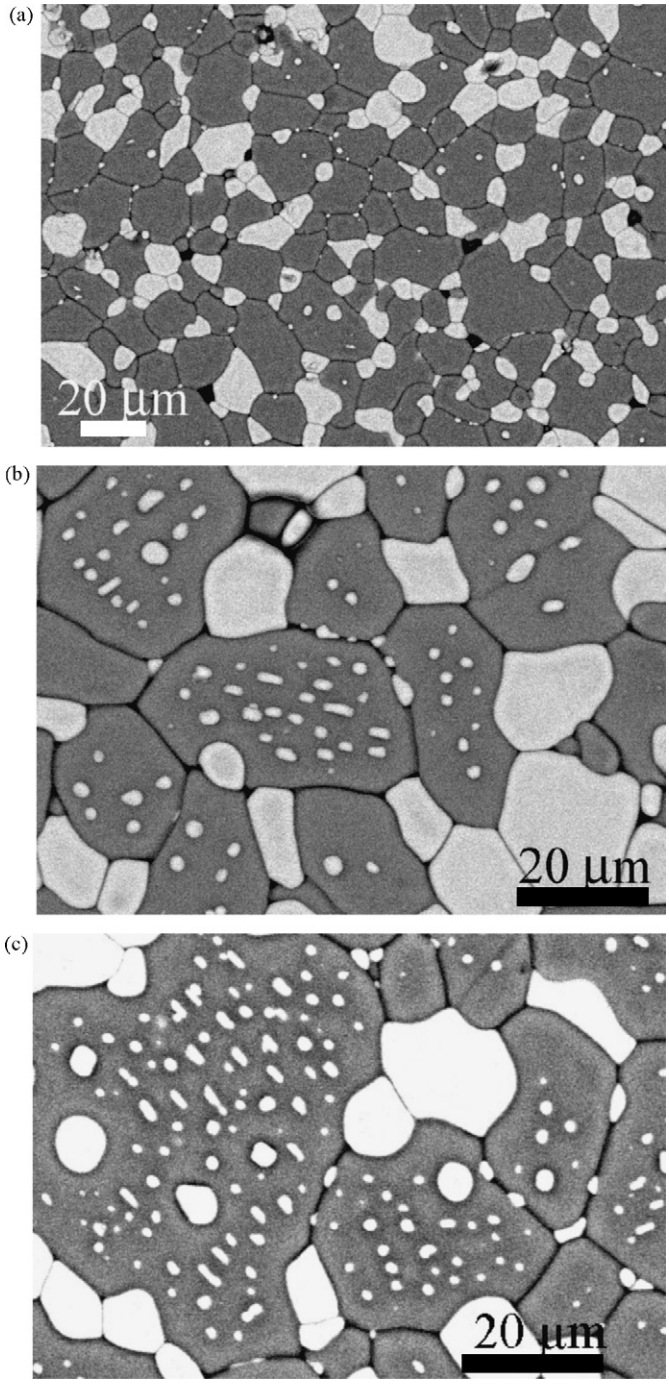

Fig. 2. SEM in back-scatted electron image mode of the Z20T80 composites fired at 1600 °C for (a) 10 h, (b) 20 h, (c) 36 h and then quenched in air; showing intragranular $ZrTiO_4$ particles became faceted and aligned by a longer annealing in (b) and (c). Sample thermally etched at 1500 °C for 10 min.

6400, 20 kV) was used to study the size and distribution of the phases in the sintered grains. Thin sections of the fired samples were Ar-ion milled to electron transparency and studied by analytical electron microscopy (AEM, JEOL 3010) at 300 kV. Transmission electron microscopy (TEM) was employed for selected area electron diffraction (SAED) pattern, bright field image (BFI), dark field image (DFI) observations of the $ZrTiO_4$ particles embedded in the Zr-dissolved TiO_2 grains. Lattice image coupled with 2D Fourier transform were used to characterize the detailed defect microstructures of the $ZrTiO_4$ particles. The relic monoclinic (m-)zirconia detected by XRD was indexed according to the distorted version of c-fluorite type parent cell.[16]

3. Results

3.1. XRD

XRD traces indicated the composites fired at 1400 °C or 1500 °C for 1 h contained rutile, $ZrTiO_4$ and residual m-ZrO_2 (Fig. 1a). The m-ZrO_2 residue was not detected for the sample fired beyond 0.5 h at 1600 °C. The rutile phase was dissolved with Zr^{4+} causing larger room temperature lattice parameters up to $a = 0.4628 \pm 0.0001$ nm, $c = 0.3001 \pm 0.0002$ nm after firing at 1600 °C for 36 h. By contrast, the $ZrTiO_4$ showed only slight change of the lattice parameters once formed at temperatures, e.g. $a = 0.4767 \pm 0.0002$ nm, $b = 0.5487 \pm 0.0002$ nm and $c = 0.5010 \pm 0.0002$ nm after firing at 1600 °C for 36 h. In general, isothermal firing of the samples at 1600 °C for 0.5 up to

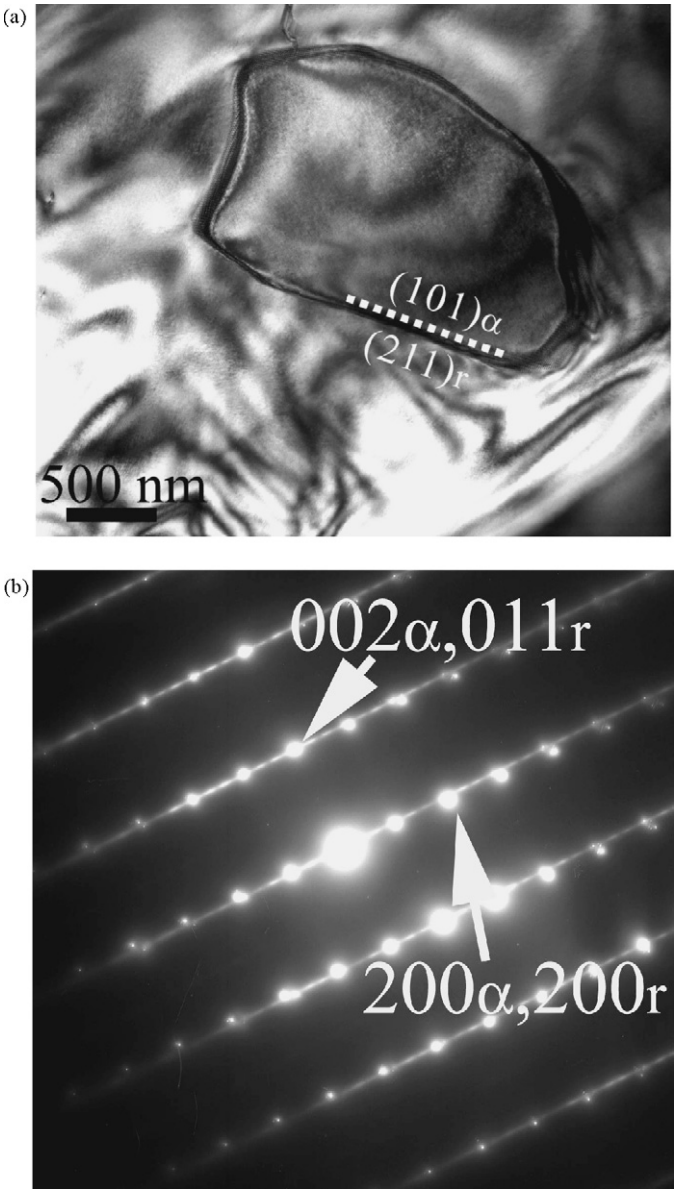

Fig. 3. TEM (a) BFI and (b) corresponding SAED pattern of an α-PbO_2-type $ZrTiO_4$ particle (denoted as α) within a host grain of rutile (denoted as r) having reached the epitaxial relationship $[0\,\bar{1}\,0]_\alpha // [0\,\bar{1}\,1]_r$; $(0\,0\,1)_\alpha // (0\,1\,1)_r$, with well developed $(1\,0\,1)_\alpha / (2\,1\,1)_r$ interface delineated by dotted line. Z20T80 sample fired at 1600 °C for 36 h and then cooled in the furnace.

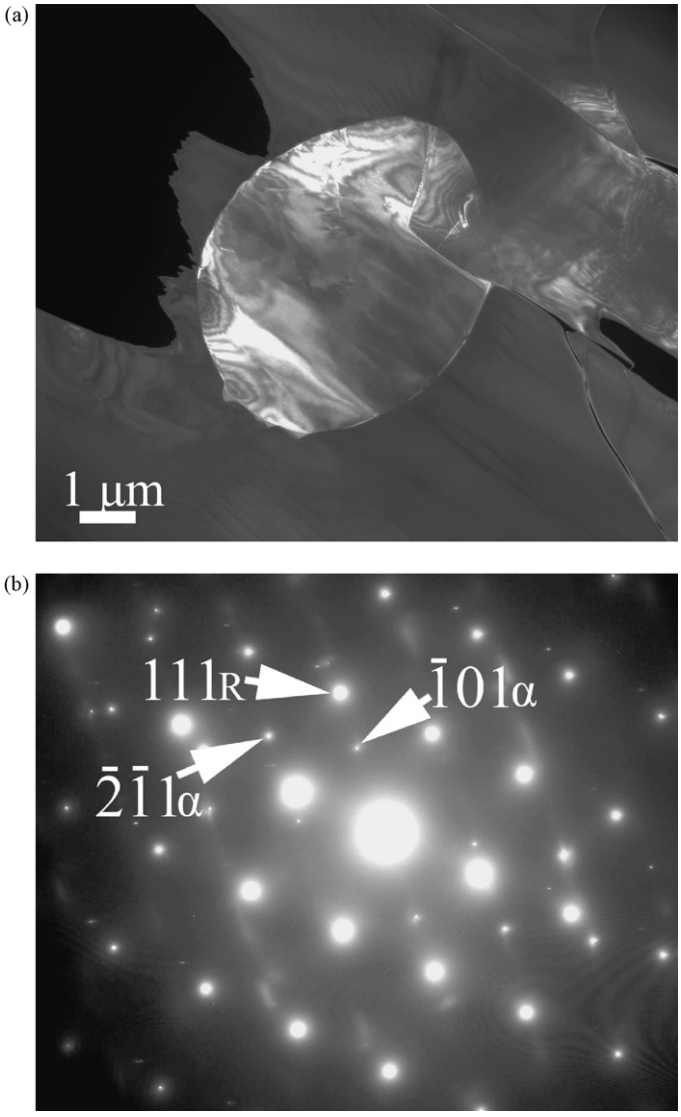

Fig. 4. TEM (a) DFI, $g = (\bar{2}\,\bar{1}\,1)_\alpha$ and (b) corresponding SAED pattern of an α-PbO_2-type $ZrTiO_4$ particle (denoted as α) approximately with a metastable epitaxial relationship $[1\,\bar{1}\,1]_\alpha // [\bar{1}\,1\,0]_r$; $(\bar{1}\,0\,1)_\alpha // (1\,1\,1)_r$ with the host rutile grain (denoted as r). Z20T80 sample fired at 1600 °C for 36 h and then quenched in air.

36 h followed by air-quenching or furnace cooling to room temperature caused only slight change of the lattice parameters for both Zr-dissolved rutile and $ZrTiO_4$.[17]

3.2. SEM

The specimens fired at 1400 °C or 1500 °C for 1 h showed $ZrTiO_4$, Zr-dissolved rutile and residual ZrO_2 as a result of incomplete reactive sintering.[17] Point-count EDX analysis revealed inward diffusion of Ti and outward diffusion of Zr for the ZrO_2 particles. The samples fired at 1600 °C for 0.5 h or 2 h have triple junctions characteristic to solid-state reactive sintering. In such samples, $ZrTiO_4$ particles were distributed mainly at grain boundaries of Zr-dissolved rutile (not shown). Further firing for 10–36 h at 1600 °C (Fig. 2) caused progressively larger rutile grains with embedded $ZrTiO_4$ particles more or less faceted i.e. having habit plane developed with respect to the host rutile grains.

3.3. TEM

The $ZrTiO_4$ particles of α-PbO_2-type structure (denoted as α) tended to reach a predominant epitaxy relationship $[0\,\bar{1}\,0]_\alpha//[0\,\bar{1}\,1]_r$; $(0\,0\,1)_\alpha//(0\,1\,1)_r$ with the host rutile grains (denoted as r) dissolved with Zr as shown representatively by the sample fired at 1600 °C for 36 h (Fig. 3). Such stable epitaxial $ZrTiO_4$ particles have a well-developed $(1\,0\,1)_\alpha/(2\,1\,1)_r$ interface. In this sample, metastable epitaxial relationship $[1\,\bar{1}\,1]_\alpha//[\bar{1}\,1\,0]_r$; $(\bar{1}\,0\,1)_\alpha//(1\,1\,1)_r$ was also observed (Fig. 4), which is related to the predominant epitaxy by pole specific rotation as discussed later.

The sample fired at 1600 °C for 0.5 h showed another metastable epitaxy relation $[2\,0\,1]_\alpha//[1\,1\,1]_r$; $(0\,\bar{1}\,0)_\alpha//(1\,1\,\bar{2})_r$ for the intragranular $ZrTiO_4$ particle as indicated by BFI and inset SAED pattern in Fig. 5a. Point-count EDX profiles across the $ZrTiO_4$/rutile interface of this particle were shown representatively in Fig. 5c. Interdiffusion was manifested by inward diffusion of Ti (ca. 3 at.%) and outward diffusion of Zr (ca.

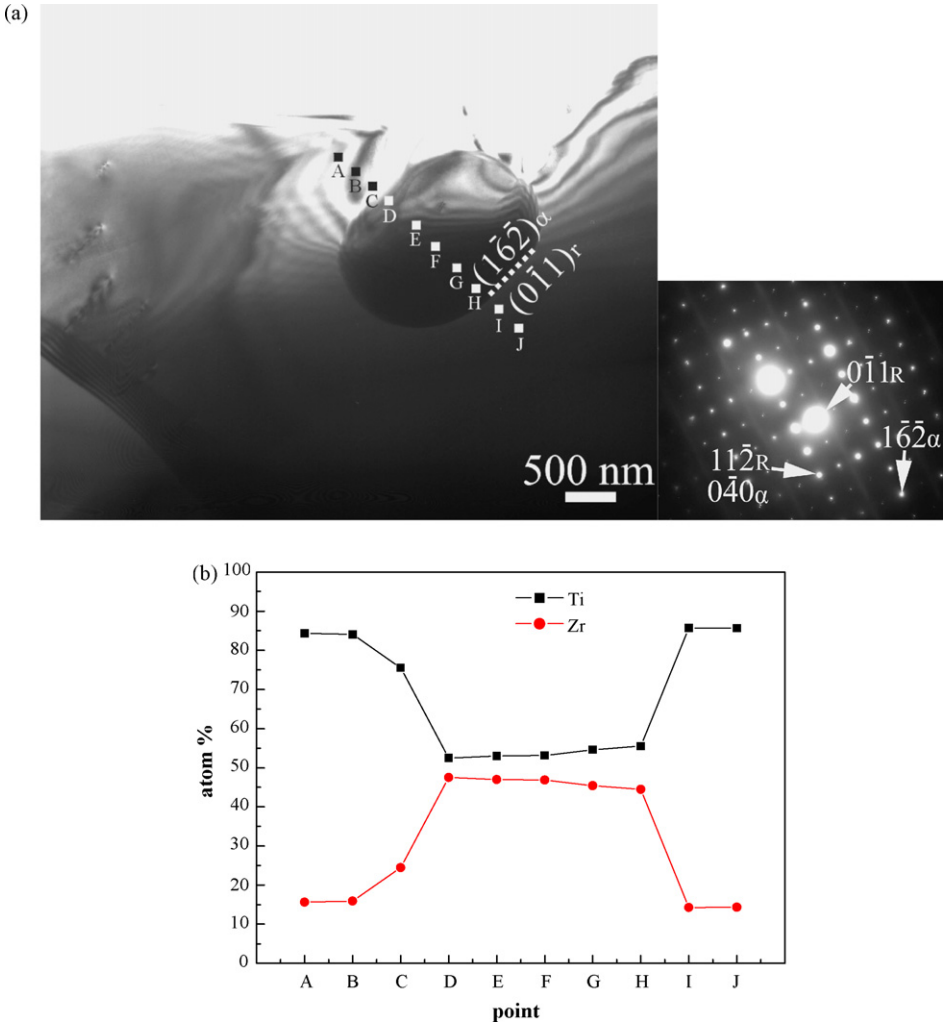

Fig. 5. TEM (a) BFI and inset SAED pattern of an intragranular $ZrTiO_4$ and rutile grain (denoted as r) in zone axis $[2\,0\,1]_\alpha$ and $[1\,1\,1]_r$, respectively having another metastable relationship $[2\,0\,1]_\alpha//[1\,1\,1]_r$; $(0\,\bar{1}\,0)_\alpha//(1\,1\,\bar{2})_r$ and apparent $(0\,\bar{1}\,1)_r/(1\,\bar{6}\,\bar{2})_\alpha$ interface. (b) point-count EDX profile (trace A–J) across the $ZrTiO_4$/rutile boundary in (a). Z20T80 sample fired at 1600 °C for 0.5 h and then air quenched.

3 at.%) against the slightly nonstoichiometric $ZrTiO_4$ particle. The intergranular $ZrTiO_4$ particles are always nonepitaxy with respect to Zr-dissolved rutile grains regardless of firing time and temperature (not shown).

The incipient exsolution of $ZrTiO_4$ particle was hardly prevented during furnace cooling, although the precipitation of $ZrTi_2O_6$ and the high to low-temperature transformation of zirconium titanate is very sluggish.[18] In fact, diffuse diffraction streaks along [0 1 1] direction were always observed for the $ZrTiO_4$ particles as represented by an intergranular one in [0 $\bar{1}$ 1] zone axis for the sample fired at 1600 °C for 36 h and then cooled in the furnace (Fig. 6). Lattice image (Fig. 7a) further showed modulated contrast parallel to (0 1 1) plane, which accounts for a set of satellite diffractions along [0 1 1] direction in the SAED pattern (Fig. 6b) and the 2D Fourier transform (Fig. 7b) from the square region in Fig. 7a. The inverse Fourier transform showed the (0 1 1) planar superlattice in 1.5 nm periodicity and dislocations with half plane parallel to (1 2 2) (Fig. 7c). Being formed upon cooling, these defects did not affect the dynamic reorientation of the intragranular $ZrTiO_4$ particles at the firing temperature 1600 °C.

4. Discussion

4.1. Reorientation of embedded nonepitaxial $ZrTiO_4$ particles in the composites

Analogous to the high-temperature dynamics of Y-PSZ particles in $Co_{1-x}O$ grains,[19] the size-dependent reorientation of the $ZrTiO_4$ particles in Zr-dissolved rutile grain can be rationalized by a Brownian-type rotation of the particles. In order to activate the Brownian motion of the embedded particles in the solid-state, a critical temperature for anchorage release (i.e. debonding) at the $ZrTiO_4$/rutile interface should occur first and in the present case it is lower than 1673 °C. This is justified by a high homologous temperature ($T/T_m = 0.92$) at 1600 °C, given the eutectic temperature 1760 °C for the binary ZrO_2–TiO_2 system.[20]

A considerable amount of vacancies due to interdiffusion of atoms across the interface is expected to benefit the anchorage release at the interface, hence facilitates particle rotation for the $ZrTiO_4$/rutile composite. This vacancy effect on debonding of atoms at interface can be further enhanced when there is considerable net vacancies flux to form Kirkendall pores under the constraint of equilibrium solid solubility at the interface. (The mutual solid solubility is about ca.15 at.% Zr in rutile and ca. 3 at.% Ti in $ZrTiO_4$ at 1600 °C according to the present EDX analysis of the composites cooled to room temperature.)

4.2. Energetics of epitaxial $ZrTiO_4$/rutile

The Brownian rotation of the intragranular $ZrTiO_4$ particles towards the predominant orientation relationship $[0\ \bar{1}\ 0]_\alpha // [0\ \bar{1}\ 1]_r$; $(0\ 0\ 1)_\alpha // (0\ 1\ 1)_r$ with respect to the rutile host, was driven by the interfacial energy cusp relevant to the planar interface of $(1\ 0\ 1)_\alpha/(2\ 1\ 1)_r$ which is characteristic of the present $ZrTiO_4$ islands in rutile (Fig. 3). This planar interface is however different from the $(0\ 0\ 1)_\alpha/(0\ 1\ 1)_r$ interface for the

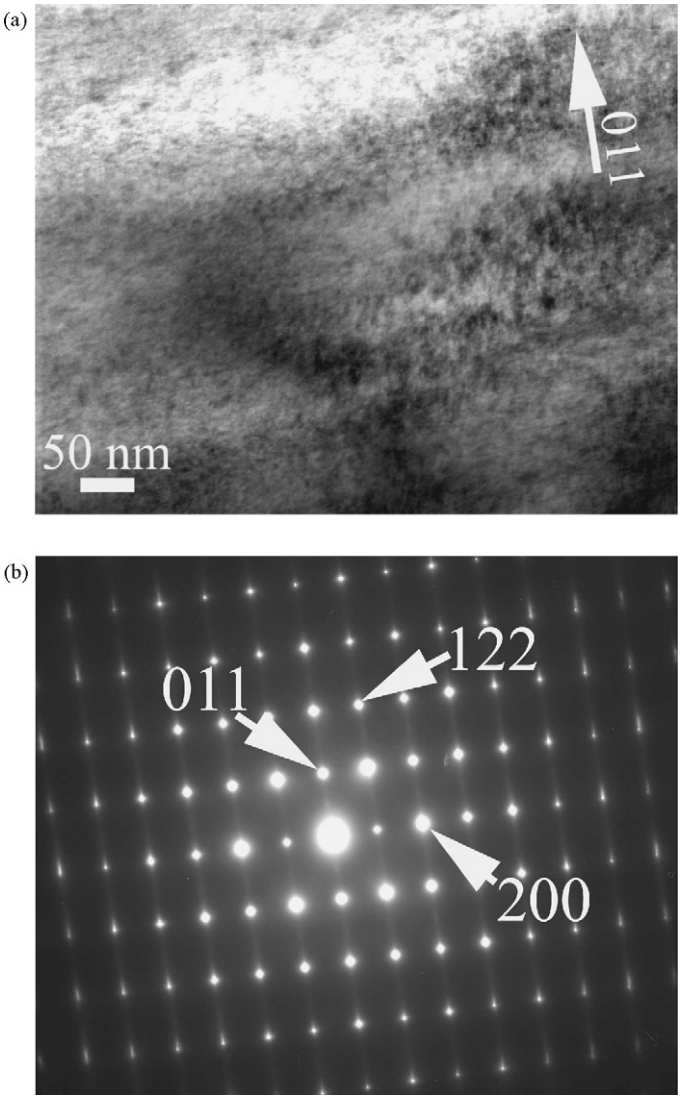

Fig. 6. TEM (a) BFI and (b) corresponding SAED pattern of the intergranular $ZrTiO_4$ grain in [0 $\bar{1}$ 1] zone axis showing diffraction streaks along [0 1 1] direction. Z20T80 sample fired at 1600 °C for 36 h and then cooled in the furnace.

natural slab of α-PbO_2-type TiO_2 at the twin boundary of rutile bicrystals in spite of the same crystallographic relationship.[21] (The present relationship $[0\ \bar{1}0]_\alpha // [0\ \bar{1}\ 1]_r$; $(0\ 0\ 1)_\alpha // (0\ 1\ 1)_r$ is the same as $[1\ 0\ 0]_\alpha // [1\ 0\ 0]_r$; $(0\ 0\ 1)_\alpha // (0\ 1\ 1)_r$ reported for natural slab.[21]) The $(0\ 0\ 1)_\alpha/(0\ 1\ 1)_r$ interface can be explained to be the habit plane of the martensitic nucleation of α-PbO_2-type TiO_2 at the (0 1 1) twin boundary of rutile already with the unit layer of α-PbO_2-type structure.[21] In fact, the structure transformation from rutile to α-PbO_2-type TiO_2 can be achieved by successive shearing of the $\{0\ 1\ 1\}$ plane of rutile.[21] To evaluate which of the two interfaces has the lower energy and is then more favored by the Brownian rotation, the oxygen planes of the $(1\ 0\ 1)_\alpha/(2\ 1\ 1)_r$ and $(0\ 0\ 1)_\alpha/(0\ 1\ 1)_r$ interfaces are plotted in Fig. 8a and b, respectively, according to the room temperature lattice parameters. The $(0\ 0\ 1)_\alpha/(0\ 1\ 1)_r$ interface turned out to have a smaller coincidence site lattice and hence more favorable than the $(1\ 0\ 1)_\alpha/(2\ 1\ 1)_r$ interface in terms of unrelaxed oxygen positions. However, in the present case $(1\ 0\ 1)_\alpha/(2\ 1\ 1)_r$ interface

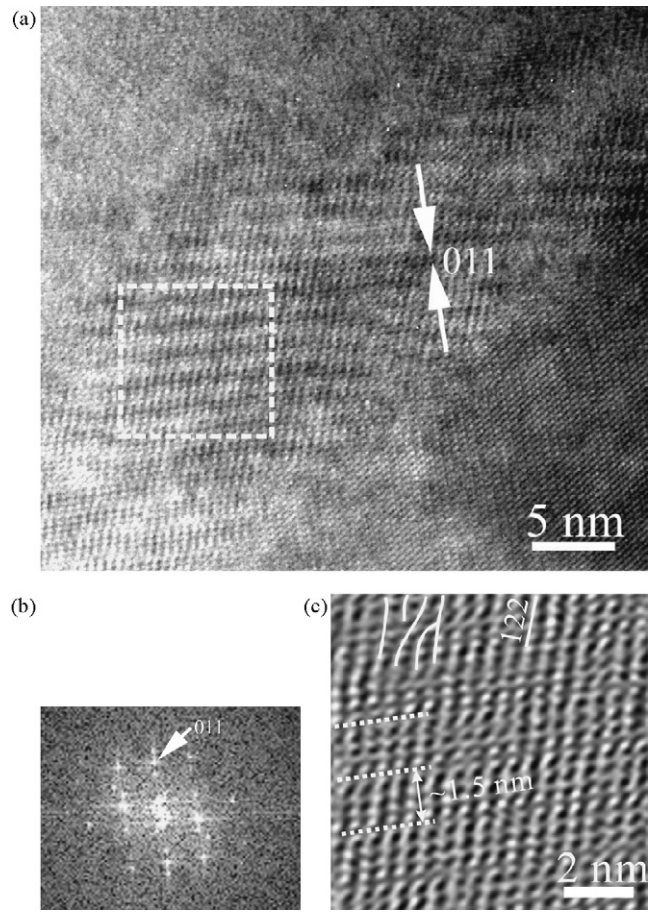

Fig. 7. (a) Lattice image of the intergranular $ZrTiO_4$ grain in $[0\,\bar{1}\,1]$ zone axis showing modulated contrast parallel to (0 1 1) plane. (b) Fourier transform from the square region in (a), showing satellite diffraction spots along [0 1 1] direction. (c) Inverse Fourier transform showing (0 1 1) planar superlattice ca. 1.5 nm in periodicity and dislocations with half plane parallel to (1 2 2).

is observed, which implies that other factors such as Coulumbic interaction and mixed strain effect may help to stabilize the $(1\,0\,1)_\alpha/(2\,1\,1)_r$ interface.

A cation–anion unmixed plane with a net dipole moment would probably be unsuitable as a boundary face of an ionic crystal. In this regard, the $ZrTiO_4$ $(0\,0\,1)_\alpha$ and rutile $(0\,1\,1)_r$ are cation–anion unmixed, whereas the $ZrTiO_4$ $(1\,0\,1)_\alpha$ and rutile $(2\,1\,1)_r$ are cation–anion mixed. The $(0\,0\,1)_\alpha/(0\,1\,1)_r$ interface thus may possess a net dipole moment in the unrelaxed state, rendering it unstable analogous to the ionic crystals.[22] In such case, a shared oxygen layer may be necessary in order to maintain charge neutrality and to minimize interfacial energy for the $(0\,0\,1)_\alpha/(0\,1\,1)_r$ interface, similar to the directionally solidified eutectic NiO/ZrO_2 (CaO) lamellae.[23] On the other hand, both planes of the planar $(1\,0\,1)_\alpha/(2\,1\,1)_r$ interface are cation–anion mixed and may be further stabilized by Coulumbic interaction energy for the $ZrTiO_4$ islands within Zr-dissolved TiO_2 host grains. It is the interface of the lowest energy and is commonly observed in the present experiment (Figs. 2 and 3).

As for the mixed strain effect, it is of interest to note that nanosize particles of α-PbO_2-type TiO_2 and rutile produced by laser ablation condensation follow another crystallographic relationship $[0\,0\,1]_\alpha//[1\,0\,0]_r$; $(1\,0\,0)_\alpha//(0\,1\,1)_r$,[24] which is different from the $[0\,\bar{1}\,0]_\alpha//[0\,\bar{1}\,1]_r$; $(0\,0\,1)_\alpha//(0\,1\,1)_r$ of the present $ZrTiO_4$ islands within Zr-dissolved TiO_2 host grains. The relationship $[0\,0\,1]_\alpha//[1\,0\,0]_r$; $(1\,0\,0)_\alpha//(0\,1\,1)_r$ was rationalized by the coalescence of the two condensates via the contact planes of $(1\,0\,0)_\alpha$ and $(0\,1\,1)_r$. Examination of this $(1\,0\,0)_\alpha/(0\,1\,1)_r$ interface shows a mixed strain effect which can reduce the interfacial energy.[24] It is therefore not apparent that the relationship $[0\,0\,1]_\alpha//[1\,0\,0]_r$; $(1\,0\,0)_\alpha//(0\,1\,1)_r$ for the coalesced condensates is indeed an energy cusp. It could be a local energy minimum relative to a small deviation of the present interface position.

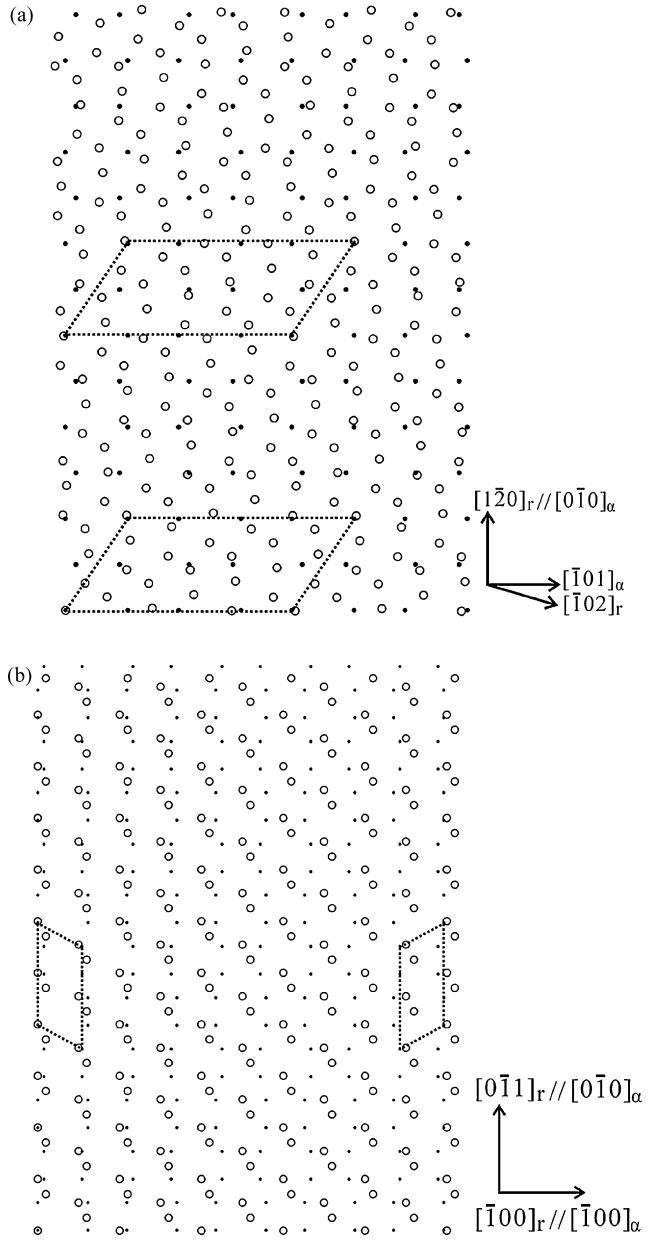

Fig. 8. Top view of the interface for α-PbO_2-type (closed circles) and rutile type (open circles) structure in terms of unrelaxed oxygen positions for the epitaxial relationship $[0\,\bar{1}\,0]_\alpha//[0\,\bar{1}\,1]_r$; $(0\,0\,1)_\alpha//(0\,1\,1)_r$, the same as $[1\,0\,0]_\alpha//[1\,0\,0]_r$; $(0\,0\,1)_\alpha//(0\,1\,1)_r$ reported for natural occurrence:[21] (a) $(1\,0\,1)_\alpha/(2\,1\,1)_r$ interface in this study; (b) $(0\,0\,1)_\alpha/(0\,1\,1)_r$ interface for natural TiO_2 polymorphs.[21] The dashes indicate the coincidence site lattice.

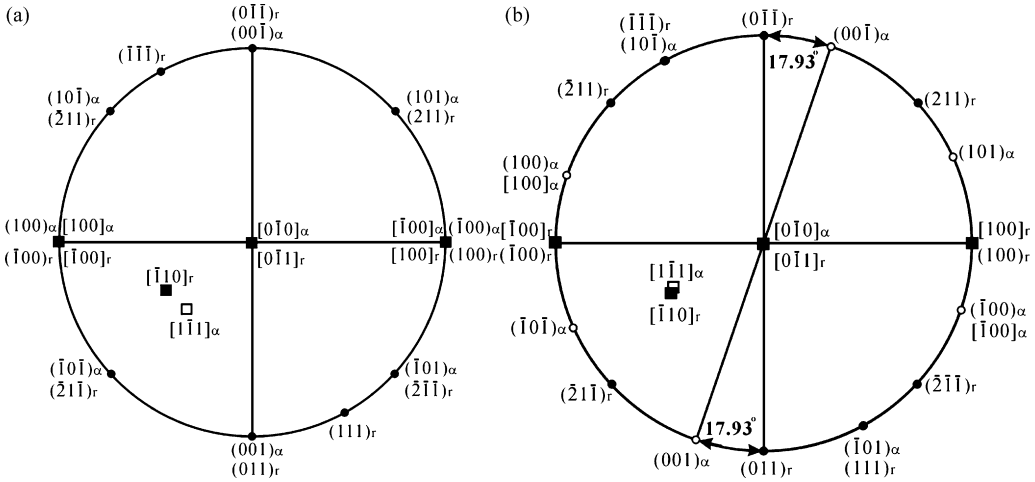

Fig. 9. Stereographic projections of the plane normals (circles) and zone axes (squares) of the intragranular $ZrTiO_4$ (denoted as α, open symbol) and the rutile host (denoted as r, solid symbol): (a) stable epitaxy $[0\,\bar{1}\,0]_\alpha//[0\,\bar{1}\,1]_r$; $(0\,0\,1)_\alpha//(0\,1\,1)_r$; (b) metastable epitaxy $[1\,\bar{1}\,1]_\alpha//[\bar{1}\,1\,0]_r$; $(\bar{1}\,0\,1)_\alpha//(1\,1\,1)_r$ which becomes stable epitaxy by clockwise or counterclockwise rotation about the $[0\,\bar{1}\,0]_\alpha/[0\,\bar{1}\,1]_r$ pole by 17.93° in order to have specific plane normals, i.e. $(0\,0\,1)_\alpha//(0\,1\,1)_r$ superimposed.

In the present composites fabricated by reactive sintering at high temperatures, in addition to the predominant relationship $[0\,\bar{1}\,0]_\alpha//[0\,\bar{1}\,1]_r$; $(0\,0\,1)_\alpha//(0\,1\,1)_r$ with the $(1\,0\,1)_\alpha/(2\,1\,1)_r$ interface, the mixed strain effect is expected to vary with complicated interdiffusion at the scale of individual $ZrTiO_4$ and rutile grains and may therefore form a metastable epitaxy such as $[1\,\bar{1}\,1]_\alpha//[\bar{1}\,1\,0]_r$; $(\bar{1}\,0\,1)_\alpha//(1\,1\,1)_r$ in Fig. 4. As shown by the stereographic projections (Fig. 9), the relation $[1\,\bar{1}\,1]_\alpha//[\bar{1}\,1\,0]_r$;$(\bar{1}\,0\,1)_\alpha//(1\,1\,1)_r$ can change into the primary crystallographic relationship $[0\,\bar{1}\,0]_\alpha//[0\,\bar{1}\,1]_r$; $(0\,0\,1)_\alpha//(0\,1\,1)_r$ by a rotation of ca. 17.93°, either clockwise or counterclockwise, about $[0\,\bar{1}\,0]_\alpha/[0\,\bar{1}\,1]_r$ pole until the $(1\,0\,1)_\alpha$ and $(2\,1\,1)_r$ planes are superimposed. However, it is by no means clear whether such a rotation over $(0\,1\,0)_\alpha$ really occurred.

As a final remark, we believe that the reorientation of the embedded $ZrTiO_4$ particles within Zr-dissolved rutile host grains can be rationalized by reactive-sintering facilitated Brownian rotation of the particles until energetically favorable interface state is reached under the combined influences of lattice mismatch, Coulumbic interactions and mixed strain effect.

Acknowledgements

We thank L.J. Wang for technical assistance on AEM. Supported by Center for Nanoscience and Nanotechnology at NSYSU and National Science Council, Taiwan, ROC, under contract NSC95-2221-E110-046. We thank the anonymous referee for constructive comments.

References

1. Chen, J. and Shen, P., On the rotation of nonepitaxial $Ni_{1-x}O$ particles within zirconia grain. *Scripta Mater.*, 1997, **37**, 1287–1294.
2. Wang, S. R. and Shen, P., Rotation-coalescence of confined particles in $Ni_{1-x}O/NiAl_2O_4$ composites. *Mater. Sci. Eng. A*, 1998, **251**, 106–112.
3. Lin, K. T. and Shen, P., Thermally activated rotation of $Co_{1-x}O$ particles within zirconia. *Mater. Sci. Eng. A*, 1999, **270**, 125–132.
4. Rankin, J. and Sheldon, B. W., In situ TEM sintering of nano-sized ZrO_2 particles. *Mater. Sci. Eng. A*, 1995, **204**, 48–53.
5. Doo, V. Y. and Balluffi, R. W., Structural changes in single crystal copper-alpha brass diffusion couple. *Acta Metall.*, 1958, **6**, 428–438.
6. Poirier, J. P., *Creep of Crystals*. Cambridge University Press, Cambridge, 1985, p. 260.
7. Masson, A., Métois, J. J. and Kern, R., Migration brownienne de cristallites sur une surface et relation avec l'épitaxie. I. Partie expérimentale. *Surf. Sci.*, 1971, **27**, 463–482.
8. Kern, R., Masson, A. and Métois, J. J., Migration brownienne de cristallites sur une surface et relation avec l'épitaxie. II. Partie théorique. *Surf. Sci.*, 1971, **27**, 483–498.
9. Métois, J. J., Gauch, M., Masson, A. and Kern, R., Migration brownienne de cristallites sur une surface et relation avec l'épitaxie. III. Cas de l'aluminium sur KCl: précisions sur le méchanisme de glissement. *Surf. Sci.*, 1972, **30**, 43–52.
10. Métois, J. J., Gauch, M., Masson, A. and Kern, R., Épitaxie: phenomène de postnucleation sur L'exemple des couches minces discontinues d'aluminium et d'or sur (1 0 0) KCl. *Thin Solid Films*, 1972, **11**, 205–218.
11. Métois, J. J., Migration brownienne de cristallites sur une surface et relation avec l'épitaxie. IV. Mobilité de cristallites sur une surface: décoration de gradins monoatomiques de surface. *Surf. Sci.*, 1973, **36**, 269–280.
12. Kuo, L. Y. and Shen, P., On the rotation of nonepitaxy crystallites on single crystal substrate. *Surf. Sci.*, 1997, **373**, L350–L356.
13. Einstein, A., In *Investigations on the Theory of the Brownian Movement*, ed. R. Fürth, Methuen, 1926, pp. 1–124 (translated from German into English by A.D. Cowper).
14. Gladstone, S., Laidler, K. and Eyring, H., *The Theory of Rate Processes*. McGraw-Hill, New York, 1941.
15. Li, M. Y., Shen, P. and Hwang, S. L., Oxidation-decomposition facilitated reorientation of nanoparticles in reactively sintered $(Ni_{0.33}Co_{0.6})_{71-\delta}O$ polycrystals. *Mater. Sci. Eng. A*, 2003, **343**, 227–234.
16. Teufer, G., The crystal structure of tetragonal ZrO_2. *Acta Crystallogr.*, 1962, **15**, 1187–1188.
17. Yang, K.C., *Defect clusters, nanoprecipitates and Brownian motion of particles in Mg-doped $Co_{1-x}O$, Ti-doped $Co_{1-x}O$, Ti-doped MgO and Zr-doped TiO_2*. Ph.D. Thesis, National Sun Yat-sen University, Taiwan, 2005.
18. McHale, A. E. and Roth, R. S., Investigation of the phase transition in $ZrTiO_4$ and $ZrTiO_4$–SnO_2 solid solutions. *J. Am. Ceram. Soc.*, 1983, **66**, C18–C20.
19. Lee, W. H. and Shen, P., Reorientation of intra- and intergranular particles in sintered Y-PSZ/$Co_{1-x}O$ composites. *Mater. Sci. Eng. A*, 2002, **338**, 253–258.
20. McHale, A. E. and Roth, R. S., Low-temperature phase relationships in the system ZrO_2–TiO_2. *J. Am. Ceram. Soc.*, 1986, **69**, 827–832.
21. Hwang, S. L., Shen, P., Chu, H. T. and Yui, T. F., Nanometer size α-PbO_2-type TiO_2 in garnet: a thermobarometer for ultrahigh-pressure metamorphism. *Science*, 2000, **288**, 321–324.

22. Tasker, P. W., The surface properties of uranium dioxide. *Surf. Sci.*, 1979, **87**, 315–324.
23. Dravid, V. P., Lyman, C. E., Notis, M. R. and Recolevschi, A., High resolution transmission electron microscopy of interphase interfaces in NiO–ZrO_2(CaO). *Ultramicroscopy*, 1989, **29**, 60–70.
24. Shen, P., Chen, S. and Tsai, M. H., Lattice correspondence of α-PbO_2-type TiO_2 and rutile. In *Proceedings of the PTM05 conference on solid–solid phase transformations in inorganic materials, Vol. 2*, ed. J. M. Home, D. E. Laughlin, J. K. Lee, U. Dahmen and W. A. Soffa, 2005, pp. 1055–1061.